Comparison of Backbone Dynamics of Reduced and Oxidized *Escherichia coli* Glutaredoxin-1 Using ^{15}N NMR Relaxation Measurements†

John J. Kelley III,‡ Thomas M. Caputo,‡ Steven F. Eaton,§ Thomas M. Laue,§ and John H. Bushweller*,‡

Department of Chemistry, Dartmouth College, Hanover, New Hampshire 03755, and Department of Biochemistry, University of New Hampshire, Durham, New Hampshire 03824

Received August 27, 1996; Revised Manuscript Received February 19, 1997⊗

ABSTRACT: NMR-based structure determination of *Escherichia coli* glutaredoxin-1 in its reduced and oxidized forms revealed only subtle structural differences between the two forms. In an effort to characterize the role dynamics may play in the functioning of the protein, the backbone dynamics of both the reduced and oxidized forms of *E. coli* glutaredoxin-1 have been characterized using inverse-detection two-dimensional ^{15}N-^{1}H NMR spectroscopy. Longitudinal (T_1) and transverse (T_2) ^{15}N relaxation time constants and steady-state {^{1}H}-^{15}N NOEs were measured for a majority of the protonated backbone nitrogen atoms. These data were analyzed by using a model-free formalism to determine the generalized order parameter (S^2), the effective correlation time for internal motions (τ_e), ^{15}N exchange broadening contributions (R_{ex}), and the overall molecular rotational correlation time (τ_m). Sedimentation equilibrium measurements showed the reduced protein to be monomeric whereas the oxidized form could be fit to a monomer−dimer equilibrium. In order to try and assess the effect of dimerization on the dynamical parameters, the measurements on the oxidized protein have been carried out at two concentrations with very different monomer/dimer ratios. There is increased motion on both nano−picosecond and micro−millisecond time scales in the reduced form relative to the oxidized form, consistent with a more rigid oxidized protein. The increase in motion in the reduced protein correlates with its decreased thermodynamic stability. The role of the observed differences in the dynamic behavior in the two forms, particularly in the active site, in glutaredoxin-1's role as a protein disulfide reductant is discussed.

Glutaredoxin-1 (Grx-1)[1] is a small protein (M_r = 12 000) involved in electron transfer reactions via the reversible oxidation of two SH groups to a disulfide bond in the active site. The active site sequence Cys-Pro-Tyr-Cys is highly conserved among a variety of different organisms including *Escherichia coli*, vaccinia virus, yeast, plants, and mammalian cells (Ahn & Moss, 1992; Gan & Wells, 1987; Gan *et al.*, 1990; Höög *et al.*, 1983; Hopper *et al.*, 1989; Johnson *et al.*, 1991; Klintrot *et al.*, 1984; Minakuchi *et al.*, 1994; Padilla *et al.*, 1995). Glutaredoxins are essential for the glutathione-dependent synthesis of deoxyribonucleotides by ribonucleotide reductase (Holmgren, 1976, 1979a; Luthman *et al.*, 1979; Luthman & Holmgren, 1982; Åslund *et al.*, 1994). Glutaredoxin-1 has inherent glutathione-disulfide oxidoreductase activity in a coupled system with GSH, NADPH, and glutathione reductase (Luthman & Holmgren, 1982), catalyzing the reduction of low molecular weight disulfides as well as proteins. A binding site for glutathione has been identified on glutaredoxin-1 (Bushweller *et al.*, 1992), providing a rationale for the preference of glutaredoxin for glutathione-containing disulfides. Grx has been proposed to exert a general thiol redox control of protein activity by acting both as an effective protein disulfide reductase (Holmgren, 1985; Ziegler, 1985) and as a specific GSH-mixed disulfide reductase. In addition, glutaredoxin catalyzes the GSH-dependent reduction of dehydroascorbate to ascorbate (Wells *et al.*, 1990; Mårtensson & Meister, 1991), suggesting a function to defend cells against oxidative stress.

The glutaredoxin family of proteins is distinguished from the thioredoxin family of proteins on the basis of their differential reactivity. Glutaredoxins are reduced by GSH (which is, in turn, reduced by GSH reductase) but not by thioredoxin reductase, whereas thioredoxins are reduced by the corresponding thioredoxin reductases but not by GSH; thus, these two families of proteins represent independent sources of reducing equivalents. In addition, glutaredoxin catalyzes GSH-disulfide oxido-reduction reactions unlike thioredoxin which acts as a quite general protein disulfide reductase (Holmgren, 1979b, 1985). Thioredoxin and glutaredoxin belong to a larger class of proteins catalyzing redox reactions in the cell. For several members of this class, three-dimensional structures have been reported, *e.g.*, for the oxidized form of *E. coli* thioredoxin by X-ray crystallography (Katti *et al.*, 1990), for the reduced form of *E. coli* thioredoxin by NMR (Dyson *et al.*, 1990; Jeng *et al.*, 1994), for the reduced form of human thioredoxin by NMR (Forman-Kay *et al.*, 1991; Qin *et al.*, 1994), for the oxidized form of T4 glutaredoxin by X-ray crystallography (Eklund *et al.*, 1992), the oxidized form of calf thymus glutaredoxin

† These studies were supported by funds provided by Dartmouth College.

* To whom correspondence should be addressed.

‡ Dartmouth College.

§ University of New Hampshire.

⊗ Abstract published in *Advance ACS Abstracts,* April 1, 1997.

[1] Abbreviations: CPMG, Carr−Purcell−Meiboom−Gill; DTT, dithiothreitol; GdmCl, guanidinium chloride; Grx, glutaredoxin; Grx-1, *E. coli* glutaredoxin-1; Grx-3, *E. coli* glutaredoxin-3; GSH, glutathione; HED, β-hydroxyethylene disulfide; kDa, kilodalton; M, moles per liter; NADPH, nicotine adenine dinucleotide phosphate; NMR, nuclear magnetic resonance; NOE, nuclear Overhauser effect; OD_{600}, optical density at 600 nm; R_1, spin−lattice or longitudinal relaxation rate constant; R_2, spin−spin or transverse relaxation rate constant; RMS, root-mean-square; SSE, sum of squares error.

S0006-2960(96)02181-2 CCC: $14.00 © 1997 American Chemical Society

by X-ray crystallography (Katti et al., 1995), and for oxidized, reduced, and glutathione mixed disulfide forms of *E. coli* glutaredoxin-1 by NMR (Xia *et al.*, 1992; Sodano *et al.*, 1991; Bushweller *et al.*, 1994).

The recent solution of the NMR structures of the reduced, oxidized, and glutathione mixed disulfide forms of *E. coli* glutaredoxin-1 has shown all three forms of the protein to be structurally very similar (Xia *et al.*, 1992; Sodano *et al.*, 1991; Bushweller *et al.*, 1994). Only subtle structural differences between the three forms were identified as has also been observed for the structures of the oxidized and reduced forms of *E. coli* thioredoxin (Dyson et al., 1990; Chandrasekhar *et al.*, 1991). Since only subtle structural differences were observed among the different forms of glutaredoxin, it is of significant interest to examine the dynamic behavior of the different forms of the protein.

The dynamics of proteins is an important element of their functional behavior. For example, protein-protein recognition processes must involve protein flexibility in order to enable the appropriate conformational changes necessary for function to take place (Bennett & Huber, 1983; Ringe & Petsko, 1985; Brooks *et al.*, 1988). *E. coli* glutaredoxin-1 presents a useful system to examine the role of dynamics in the function of a protein disulfide reductase. Since the redox potential of this protein is determined by the overall thermodynamic stability of the two forms and the structural differences between the reduced and oxidized forms of the protein are quite subtle, the dynamics are likely to play a role in the differential stability of the two forms. Additionally, in its role as a protein disulfide reductant, the reduced form of the protein will bind to protein disulfide substrates whereas the oxidized form dissociates. Since the structural differences are small between the two forms, it is also likely that any differential dynamic behavior between the two forms also plays a role in the interaction of the protein with its protein disulfide substrates.

The backbone dynamics of a large number of proteins have been characterized by NMR spectroscopy [for reviews, see Palmer (1993), Wagner (1993)], but only a few of these studies have focused on catalytically active enzymes. A previous study of the backbone dynamics of reduced and oxidized *E. coli* thioredoxin revealed relatively few differences between the two forms of the protein that were limited to the micro−millisecond time scale and were localized to the vicinity of the active site (Stone *et al*., 1993). Comparison of the dynamics of the reduced and oxidized forms of glutaredoxin reveal significant dynamical differences in the active site and in residues spatially close to the active site. These differences correlate well with the known higher thermodynamic stability of the oxidized protein.

EXPERIMENTAL PROCEDURES

Sample Preparation. E. coli Grx-1 was expressed in *E. coli* AR58 cells from the plasmid p-AHOB1 as described previously (Björnberg & Holmgren, 1991). For ^{15}N-labeling of the protein, cells were grown in M9 minimal media supplemented with (1 mg/L biotin, 1 mg/L thiamine, 10 g/L glucose, 8 g/L $(^{15}NH_4)_2SO_4$, 1 mM $MgSO_4$, 0.3 mM $CaCl_2$, 0.3 mM Na_2SO_4, 0.5 g/L NaCl, 2.0 g/L KH_2PO_4, 8.0 g/L Na_2HPO_4, 100 μg/mL carbenicillin, and 10 mL of a trace elements solution containing $FeCl_3$, $ZnCl_2$, $CuCl_2$, $CoCl_2 \cdot 6H_2O$, H_3BO_3, and $MnCl_2 \cdot 6H_2O$. Typically, 1 L of cells was grown at 29 °C with shaking at 250 rpm until the OD_{600} reached a value of 2.0. The cells were then centrifuged at 4000 rpm for 15 min. The resulting cell pellet was resuspended in an equal volume of fresh media, the cells were allowed to recover for 30 min at 29 °C, then the temperature was raised to 40 °C to induce protein production for an additional 8 h. The protein was purified according to the procedure described in Bushweller et al. (1992) with the exception that DTT was left out of all buffers. The protein was exchanged into the buffer used for the NMR experiments [50 mM potassium phosphate (pH 6.5), 0.1 mM EDTA, 0.1% sodium azide, and 5 mM DTT for the reduced protein] by buffer exchange on a column of Sephadex G25 (Pharmacia). NMR samples contained 2.3 mM Grx-1 in 525 μL of the above buffer containing 5% D_2O.

Sedimentation Equilibrium. Short column (Yphantis, 1960; Laue, 1992) and high-speed (Yphantis, 1964) equilibrium experiments were conducted at 20 °C in a Beckman XL-l ultracentrifuge at eight rotor speeds between 14 000 and 40 000 rpm using interference detection. For each sample, three or four cell loading concentrations were examined going from 0.09 to 1 mg/mL in 50 mM potassium phosphate (pH 6.5), 0.1 mM EDTA, plus 1 mM DTT for the reduced protein. Data were fit using NONLIN (Johnson et al., 1981), with the selection of models and conversion of units as described previously (Laue, 1995). Partial specific volumes and solvent densities were calculated as described (Laue et al., 1992). The calculated partial specific volume (0.728 mL/g) was adjusted for the peptide charge (−4 at pH 7.5) by decreasing the molar volume 25 mL/mol to 0.718 mL/g. An additional uncertainty of ±0.005 in the partial specific volume was included when calculating the molecular weight (Kharakoz, 1989; Starovasnik et al., 1992).

NMR Spectroscopy. All NMR spectroscopy was carried out at 25 °C on a Varian UnityPlus 500 MHz NMR spectrometer equipped with an actively shielded broadband inverse detection probe and pulsed field gradients. T_1, T_2, and NOE measurements for the 0.48 mM oxidized sample were recorded on a Nalorac 5 mm triple resonance pulsed field gradient probe. The pulse sequences of Farrow et al. (1994) optimized for minimal saturation of water were employed for recording of the T_1, T_2, and heteronuclear NOE values. For all experiments, spectral widths of 1600 Hz (^{15}N) and 6500 Hz (^{1}H) were employed with the carriers set at 115 and 4.74 ppm, respectively. All spectra were recorded as 128* × 1024* complex matrices with 24 scans per t_1 point.

For the T_1 and T_2 measurements, a recycle delay of 1.5 s was used between acquisitions to ensure sufficient recovery of ^{1}H magnetization (Sklenar et al., 1987). ^{15}N T_1 values were measured from spectra recorded with eight different durations of the delay: 44.5, 122.3, 244.6, 500.4, 745, 1245.4, 2001.6, and 3002.4 ms for Grx-$(SH)_2$; 44.5, 122.3, 244.6, 500.4, 756.1, 1267.6, 1823.5, and 3024.4 ms for 2.3 mM Grx-S_2; and 44.5, 122.3, 244.6, 500.4, 756.1, 1000.8, 1501.2, and 2502.0 ms for 0.48 mM Grx-S_2. ^{15}N T_2 values were measured from spectra recorded with delays corresponding to the duration of the CPMG sequence: 16.3, 32.6, 48.9, 97.7, 130.3, 195.5, 309.5, 407.2, and 651.5 ms for Grx-$(SH)_2$; 16.3, 32.6, 48.9, 65.2, 81.4, 97.7, 130.3, 179.2, 325.8,

and 456.1 ms for 2.3 mM Grx-S_2; and 16.2, 32.4, 48.6, 64.8, 81.0, 97.1, 129.5, 178.1, 307.6, 453.3, and 599.0 for 0.48 mM Grx-S_2. To permit estimation of noise levels as well as to improve the accuracy of the data, duplicates of every other time point were recorded [44.5, 244.6, 756.1, and 1823.5 ms for 2.3 mM Grx-S_2 T_1 and 16.3, 48.9, 81.4, and 130.3 ms for 2.3 mM Grx-S_2 T_2; 44.5, 244.6, 756.1, and 1501.2 ms for 0.48 mM Grx-S_2 T_1 and 16.2, 48.6, 81.0, and 129.5 ms for 0.48 mM Grx-S_2 T_2; 44.5, 244.6, 745, and 2001.6 ms for Grx-$(SH)_2$ $T_1$and 16.3, 48.9, 130.3, and 309.5 ms for Grx-$(SH)_2$ T_2]. NOE values were determined from spectra recorded in the presence and absence of a proton presaturation period of 3 s within a total recycle delay of 5 s between acquisitions. As described by Farrow *et al*. (1994), ^{1}H saturation was achieved by application of 120° ^{1}H pulses every 5 ms throughout the presaturation period.

Data Processing and Analysis. In order to generate pure absorptive 2D line shapes, the N- and P-type signals recorded for each t_1 point were stored separately in order to carry out the necessary addition and subtraction of FIDs and 90° phase correction as previously described (Kay et al., 1992). The necessary data manipulations were carried out using software written in-house. All other data processing was carried out using the program PROSA (Güntert et al., 1992). All spectra were processed identically with a Lorentz−Gauss transformation in the ω_1 and ω_2 dimensions, respectively.

The intensities of the peaks in the 2D spectra were analyzed by measuring the peak heights using the integration routine in the program XEASY (Bartels et al., 1995). The uncertainty in the peak heights in the T_1 and T_2 spectra was calculated as $\sigma_h/(2)^{1/2}$, where σ_h is the standard deviation of the differences in peak heights for pairs of duplicate spectra (Skelton et al., 1993). The pair of duplicate spectra in both the T_1 and T_2 series that displayed the largest variation was chosen for this calculation.

The T_1 and T_2 values were determined by fitting the measured peak heights to the following expression:

$$I(t) = I_0 \exp\left(-\frac{t}{T_{1,2}}\right) \quad (1)$$

in which $I(t)$ is the intensity at time t and I_0 is the intensity at time zero. T_1 and T_2 values and uncertainties were determined by nonlinear least-squares fitting of the experimental data points to the monoexponential decay given in eq 1 using the routines described previously (Palmer et al., 1991). The goodness-of-fit of the data to eq 1 was evaluated by comparison of the calculated χ^2 value with tabulated values of χ^2 at 95% confidence level as previously described (Palmer et al., 1991).

The values for the steady-state NOEs were calculated from the ratio of peak heights in the spectra recorded with and without proton saturation. The standard deviation of the NOE value was determined based on the measured background noise levels as described in Farrow et al. (1994).

The T_1 and T_2 relaxation times and the NOE enhancement of an amide ^{15}N nucleus at high field are dominated by the dipolar interaction with the directly attached NH proton and by chemical shift anisotropy (Abragam, 1961):

$$1/T_1 = (d^2/4)[J(\omega_H - \omega_N) + 3J(\omega_N) + 6J(\omega_H + \omega_N)] + c^2 J(\omega_N) \quad (2)$$

$$1/T_2 = (d^2/8)[4J(0) + J(\omega_H - \omega_N) + 3J(\omega_N) + 6J(\omega_H) + 6J(\omega_H + \omega_N)] + (c^2/6)[4J(0) + 3J(\omega_N)] + R_{ex} \quad (3)$$

$$\mathrm{NOE} = 1 + (d^2/4R_1)(\gamma_H/\gamma_N)[6J(\omega_H + \omega_N) - J(\omega_H - \omega_N)] \quad (4)$$

in which $d = (\mu_o \hbar \gamma_H \gamma_N / 8\pi^2)\langle r_{NH}^{-3}\rangle$, $c = \omega_N \Delta\sigma/(3)^{1/2}$, μ_o is the permeability of free space, $\hbar$ is Planck's constant, γ_H and γ_N are the gyromagnetic ratios of ^{1}H and ^{15}N, r_{NH} = 1.02 Å, ω_N and ω_H are the Larmor frequencies of ^{1}H and ^{15}N, and $\Delta\sigma = -160$ ppm is the chemical shift anisotropy measured for ^{15}N nuclei in helical polypeptide chains (Hiyama et al., 1988). The amplitudes and time scales of motions within the protein can be determined from the relaxation data using the model-free formalism developed by Lipari and Szabo (1982a,b) and extended by Clore and co-workers (Clore et al., 1990b). This formalism employs a minimal number of parameters to describe the overall tumbling of the protein and the internal motions of the NH vector. The spectral density function $J(\omega)$ is modeled as

$$J(\omega) = \frac{2}{5}\left[\frac{S^2\tau_m}{1 + (\omega\tau_m)^2} + \frac{[1 - (S_f)^2]\tau_f}{1 + (\omega\tau'_f)^2} + \frac{[(S_f)^2 - S^2]\tau'_s}{1 + (\omega\tau'_s)^2}\right] \quad (5)$$

where $\tau'_f = \tau_f\tau_m/(\tau_f + \tau_m)$, $\tau'_s = \tau_s\tau_m/(\tau_s + \tau_m)$, τ_m is the overall rotational correlation time of the molecule, τ_f is the internal correlation time for internal motions on a rapid time scale (τ_f < 100−200 ps), τ_s is the effective correlation time for internal motions on a slower time scale ($\tau_f < \tau_s < \tau_m$), $S^2 = S_f^2 S_s^2$ is the square of the generalized order parameter characterizing the amplitude of the internal motions, where S_f^2 and S_s^2 are the squares of the order parameters for the internal motions on the fast and slow time scales. The order parameter S^2 describes the degree of spatial restriction of the internal motion of the NH bond vector. An R_{ex} term is also included in eq 3 to account for contributions to the transverse relaxation rate from chemical exchange or other processes that contribute to the decay of transverse magnetization. As has been done previously (Mandel et al., 1995), motions described by the generalized order parameter will be referred to as pico−nanosecond dynamics and motions described by the R_{ex} term will be referred to as micro−millisecond time scale dynamics.

As described in Mandel et al. (1995), five models consisting of subsets of the extended model-free parameters were employed for fitting to the experimental data: (a) S^2, (b) S^2, $\tau_e = \tau_f$, (c) S^2, R_{ex}, (d) S^2, $\tau_e = \tau_f$, R_{ex}, and (e) S_f^2, S^2, $\tau_e = \tau_s$. Model-free parameters were calculated from the measured relaxation parameters using the program Modelfree (version 3.1) (Palmer et al., 1991). An initial estimate of the correlation time for the reduced and oxidized forms of glutaredoxin was obtained from a 10% trimmed mean of the

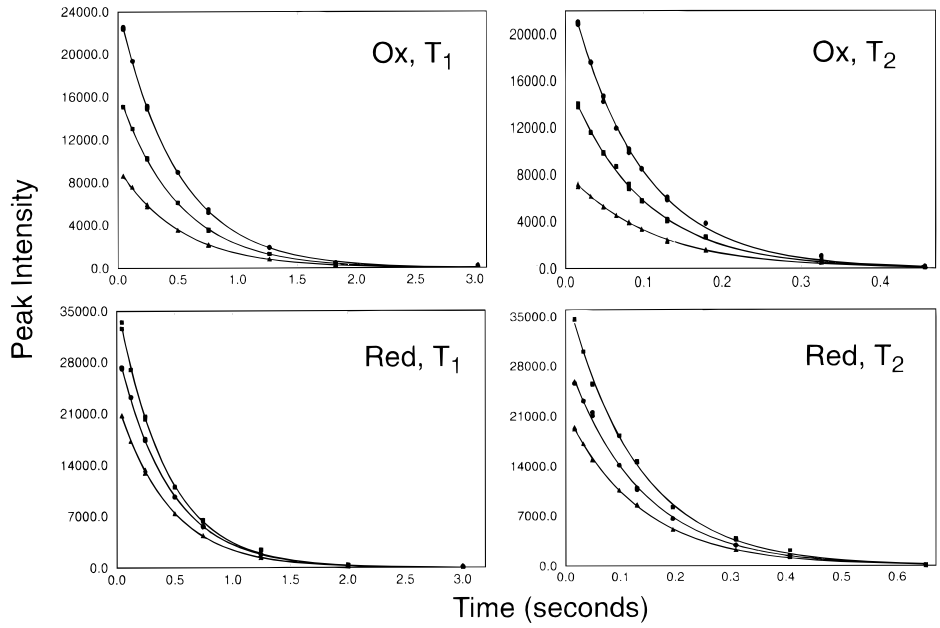

FIGURE 1: Selected T_1 (left panels) and T_2 (right panels) relaxation curves for 2.3 mM oxidized (Ox) and reduced (Red) glutaredoxin. The curves indicate best fits to single-exponential decays. Experimental data points for N26 (squares), R39 (circles), and G70 (triangles) are shown.

T_1/T_2 ratio (Kay et al., 1989) for those backbone amides with T_1 and T_2 values deemed adequate by the goodness-of-fit analysis described above. A grid search as implemented in the Modelfree program was utilized to obtain initial estimates for the values of the other model-free parameters. The optimization was carried out using the Modelfree program as described previously (Mandel et al., 1995).

Model Selection. The model selection strategy outlined by Palmer and co-workers (Mandel et al., 1995) was employed for selection of appropriate models for the fitting of each residue. The five models were initially fit to the experimental data using the estimate of τ_m obtained from the 10% trimmed mean of the T_1/T_2 ratio. In each case, 500 randomly distributed synthetic data sets were generated using Monte Carlo simulations to determine the cumulative probability distribution and the $\alpha = 0.10$ critical value of the sum of squares error. Subsequently, the simulated data generated from one model were fit using a second model with an additional parameter or parameters. The results of this simulation were employed to determine the cumulative probability distribution as well as the $\alpha = 0.20$ critical value of an F-statistic. As described in Mandel et al. (1995), a parsimonious selection of models was employed in which the simplest possible model that adequately describes the data was selected in each case. The sum of squares error was evaluated relative to the $\alpha = 0.10$ critical value obtained for a specific model from the synthetic data sets. If the value fell within this range, that model was selected. If this value was found to be out of the acceptable range, models with one additional parameter were evaluated. Again, the sum of squares error was evaluated, but in addition, an F-statistic was evaluated to determine if the addition of an additional parameter to the model had provided a statistically significant improvement to the fitting of the data. As we have only collected T_1, T_2, and NOE data at a single field strength, this statistical approach is not appropriate for models containing three parameters. Residues were fit with these three parameter models only if the sum of squares error was significantly larger than the $\alpha = 0.10$ critical value for both the one and two parameter models (generally sum of squares error > 18) and the sum of squares error for the three parameter model was zero.

RESULTS

Relaxation Parameters. Measurements were originally carried out on 2.3 mM samples of both oxidized and reduced Grx-1. Subsequently, an additional data set was collected for the oxidized form of the protein at a concentration of 0.48 mM for reasons discussed below. Single-exponential two-parameter decay functions of the form given in eq 1 were fit to the experimental decay data. For the T_1 and T_2 measurements on the reduced form of the protein, χ^2 values indicated an adequate fit for both relaxation parameters for 63 residues. For the 2.3 and 0.48 mM oxidized form of the protein, this analysis yielded 69 residues for the former and 66 residues for the latter with adequate T_1 and T_2 fits. Plots of the experimental data points and the decay curves obtained from the fitting procedure for the T_1 and T_2 data for several residues in the 2.3 mM reduced and oxidized samples of the protein are shown in Figure 1.

The values of the T_1, T_2, and NOE relaxation parameters are shown in Figure 2 for residues 2−83 for which adequate fits were obtained. T_1, T_2, and NOE values were obtained for residues 84 and 85 at the C-terminus of the protein; however, adequate fits were not obtained because of the much larger T_2 and T_1 values for these residues than for the remainder of the protein. This is in agreement with the observation in the structures of both reduced and oxidized glutaredoxin-1 that these residues are flexible (Xia et al., 1992; Sodano et al., 1991). Reliable values were not obtained for Gln66 because of severe line broadening of this residue. Average T_1 and T_2 values of 510 ± 20 and 96 ± 11 ms, respectively, were obtained for the 2.3 mM oxidized form of the protein. In the case of the T_1 values, six residues fall more than 1 standard deviation below the mean including Ile5, Cys14, Gln34, Lys45, Asp65, and Phe75. Nine residues have T_1 values falling more than 1 standard deviation above

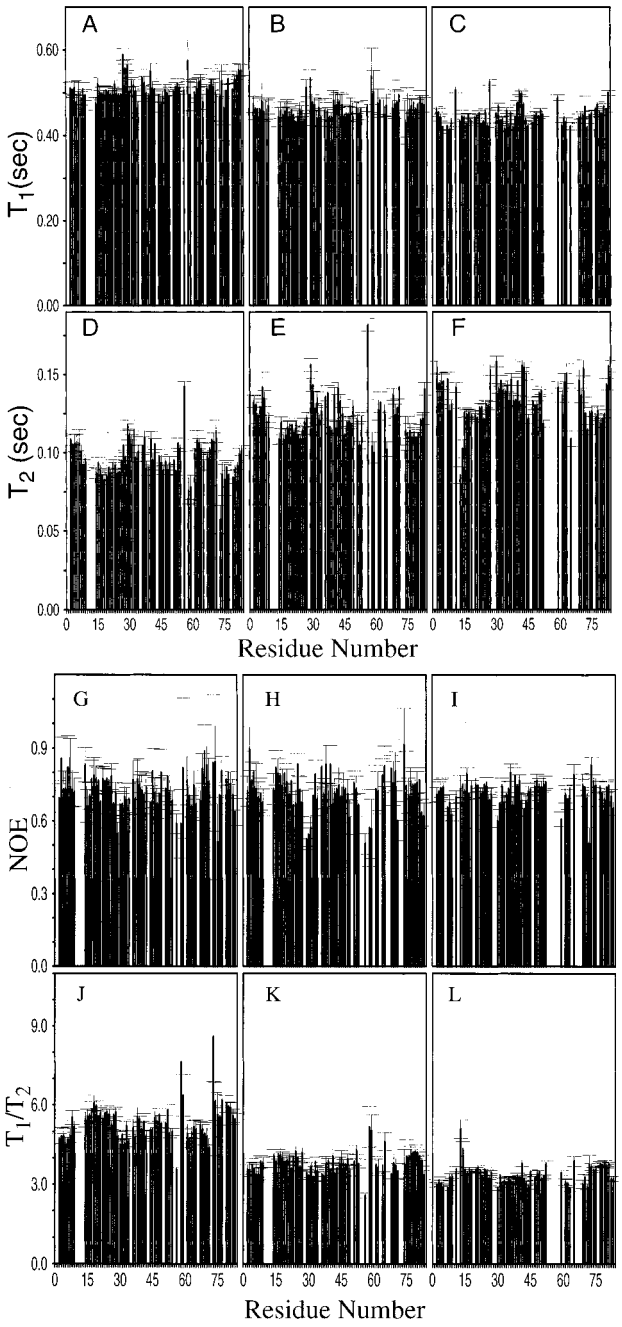

FIGURE 2: (A) Plots of T_1 and T_2 as a function of the resolved backbone NH groups in oxidized and reduced glutaredoxin: top panel shows measured T_1 values for 2.3 mM oxidized (A), 0.48 mM oxidized (B), and reduced (C) glutaredoxin; second panel shows measured T_2 values for 2.3 mM oxidized (D), 0.48 mM oxidized (E), and reduced (F) glutaredoxin. (B) Plots of $\{^1H\}$-^{15}N NOE and T_1/T_2 ratios as a function of the resolved backbone NH groups in oxidized and reduced glutaredoxin: top panel shows $\{^1H\}$-^{15}N NOEs for 2.3 mM oxidized (G), 0.48 mM oxidized (H), and reduced (I) glutaredoxin; bottom panel shows T_1/T_2 ratios for 2.3 mM oxidized (J), 0.48 mM oxidized (K), and reduced (L) glutaredoxin.

the mean including Glu27, Arg28, Asp29, Val36, Ala40, Thr58, Glu81, Asn82, and Leu83. For the T_2 values, seven residues fall more than 1 standard deviation below the mean including Lys18, Asp19, Thr58, Val59, Thr73, Phe75, and Val79. There are six residues displaying values more than 1 standard deviation above the mean including Asp29, Asp30, Gln32, Asp37, Val56, and Gly71.

For the 0.48 mM oxidized Grx-1 sample, mean T_1 and T_2 values of 466 ± 2 and 123 ± 14 ms, respectively, were obtained. Ten residues display T_1 values more than 1 standard deviation below the mean T_1 value including Cys14, Glu22, Lys23, Asn26, Gln32, Gln34, Ile38, Arg39, Lys45, and Asp74. Six residues displayed T_1 values more than 1 standard deviation above the T_1 mean value including Glu27, Asp29, Thr58, Val59, Gly71, and Glu81. For the T_2 values, eight residues yielded values more than 1 standard deviation below the mean T_2 value: Cys14, Arg16, Leu24, Ala52, Thr58, Val59, Asp65, and Val79. Nine residues displayed T_2 values more than 1 standard deviation above the mean: Phe6, Asp29, Asp30, Asp37, Gly42, Val56, His68, Gly71, and Leu83.

For the reduced form of the protein, mean T_1 and T_2 values of 450 ± 20 and 130 ± 10 ms, respectively, were obtained. Eleven residues display T_1 values more than 1 standard deviation below the mean T_1 value including Ile5, Gly7, Arg8, Asn26, Gln34, Val36, Ile38, Lys45, Gln61, Asp65, and Thr73. Eight residues displayed T_1 values more than 1 standard deviation above the T_1 mean value including Cys11, Glu27, Ala40, Glu41, Gly42, Val59, Trp78, and Leu83. For the T_2 values, six residues yielded values more than 1 standard deviation below the mean T2 value: Tyr13, Cys14, Ala52, Asp65, Thr73, and Val79. Nine residues displayed T_2 values more than 1 standard deviation above the mean: Gln2, Glu27, Asp30, Gly42, Ile43, Thr44, Phe63, Gly71, and Leu83.

Comparison of the T_1 and T_2 values for the 2.3 mM samples of the two forms of the protein shows a modest overall increase in T_1 and a significant decrease in T_2 on going from the reduced to oxidized forms of the protein indicative of differing overall correlation times for the two forms of the protein.

The results of the NOE measurements are also shown in Figure 2 for those residues among amino acids 2−83 for which measurements were obtained. Both residues Asp84 and Ala85 displayed depressed values of the steady-state NOE indicative of their flexibility in solution (see Supporting Information). Ala85 was the only residue to exhibit a negative NOE, clearly indicating it is very flexible in solution. A mean value of 0.74 ± 0.06 was obtained for the steady-state NOE in the 2.3 mM oxidized sample. For this form of the protein, seven residues exhibit NOE values more than 1 standard deviation below the mean (residues Asp84 and Ala85 were not included in calculation): Val15, Asp29, Val56, Thr58, Phe63, Phe75, and Leu83. Ten residues exhibited NOE values more than 1 standard deviation above the mean including Thr3, Phe6, Gly7, Cys14, Val59, His68, Ile69, Gly70, Thr73, and Asp74. For the 0.48 mM oxidized sample, a mean steady-state NOE of 0.73 ± 0.08 was measured. For this lower concentration oxidized sample, a total of ten residues show a steady-state NOE more than 1 standard deviation below the mean (residues Asp84 and Ala85 were not included in calculation): Asp29, Asp30, Phe31, Gln49, Val56, Thr58, Val59, Gly71, Asn82, and Leu83. Nine residues display NOE values more than 1 standard deviation above the mean: Thr3, Val15, Ser25, Val36, Ile38, Ala40, Asp65, His68, and Asp74. For the reduced from of the protein, a mean steady-state NOE of 0.72 ± 0.05 was obtained. For the reduced form, a total of seven residues show steady-state NOEs more than 1 standard deviation below the mean (residues Asp84 and Ala85 were not included in calculation): Gly7, Ser9, Asp30, Gly42, Val59, Tyr72, and Leu83. Five residues display NOE values

more than 1 standard deviation above the mean value: Arg16, Val36, Ile38, Asp65, and Thr73.

Overall Correlation Time τ_m. The spectral density function employed in the model-free analysis assumes isotropic tumbling of the protein. In order to assess the validity of this assumption for Grx-1, we have calculated the principal moments of inertia from the NMR solution structures of the two forms of the protein. These were found to be in the ratio of 1.00/0.92/0.52 and 1.00/0.91/0.53 for the reduced and oxidized forms of the protein, respectively. Approximating the protein as an oblate ellipsoid with axial ratios of 1.39 and 1.37 (calculated as the ratio of the long to short semiaxes) for the reduced and oxidized proteins, respectively, yielded the following values for the Perrin shape factors: $F_a = 1.15$ and $F_b = 0.996$ for the reduced protein, $F_a = 1.15$ and $F_b = 0.994$ for the oxidized form. A ratio of 1.08 is then obtained for the rotational correlation times about the long and short axes. This strongly suggests that the assumption of isotropic rotation is appropriate in this case.

Estimates of the overall correlation time can be obtained from the ratio of the T_1 and T_2 values as described earlier (Kay et al., 1989). As seen in Figure 2, the values of this ratio are relatively uniform for both forms of the protein with some clear exceptions. In order to avoid including those residues that clearly deviate from the average behavior of the protein, a 10% trimmed mean of the T_1/T_2 values was employed for the estimation of τ_m in each case. The average calculated τ_m was 5.77 ± 0.04 ns for the reduced form of the protein, 6.37 ± 0.04 for the 0.48 mM oxidized sample, and 7.96 ± 0.05 ns for the 2.3 mM oxidized sample. These values were employed in the initial grid searches of the model-free parameters. Once final models had been selected for each residue, τ_m was optimized in the final model-free calculation along with the appropriate model-free parameters for each residue. The final optimized values of the overall correlation time for the reduced sample, 0.48 mM oxidized sample, and 2.3 mM oxidized sample was 5.73 ± 0.02, 6.37 ± 0.03, and 7.95 ± 0.03 ns, respectively.

The overall correlation time of an isotropically tumbling molecule should be proportional to its volume (Cantor & Schimmel, 1980; Venable & Pastor, 1988). The very modest structural changes associated with the reduction of the disulfide should not change the volume of the protein to any significant extent and therefore do not explain the significant difference in the overall correlation times obtained for the two forms of the protein. In order to address this discrepancy, we have measured the oligomerization state of the two forms of the protein using equilibrium sedimentation.

Equilibrium Sedimentation. Reduced and oxidized Grx-1 behaved differently in sedimentation equilibrium analysis. Reduced Grx-1 sediments as a single ideal species with an apparent molecular mass of 12 300 ± 600 kDa (95% confidence interval, root mean square of the fit = 0.02 fringe). This is larger than the expected molecular mass of 9700 kDa. These data showed no change in molecular weight with either rotor speed or loading concentration, indicating that this is not due to a mass action association or contamination of the sample with aggregated material (Yphantis, 1964; Laue, 1995). Furthermore, none of the data could be fit by any model that included self-association. We conclude, therefore, that reduced Grx-1 is monomeric under these conditions. The reason for the discrepancy in molecular weight is not understood at this time. Oxidized Grx-1 did exhibit a mass action association which could be modeled adequately as a weak ideal monomer−dimer equilibrium. The model returned a monomer molecular weight of 9500 ± 500 kDa with an association constant of 1025 ± 200 M.

Model-Free Analysis. The relaxation parameters for each residue were fit using the appropriate spectral density function as determined in preliminary calculations as described by Mandel et al. (1995). All residues could be fit adequately to one of the five models. Because of the known influence of dimerization on the dynamical parameters obtained in this manner (Schurr et al., 1994), a complete analysis of the oxidized protein was also carried out from data obtained on a 0.48 mM sample where the fraction of protein in monomeric form is 62% relative to the 37% value for the original 2.3 mM sample.

Table 2 shows the distribution of residues among the five models employed for each form of the protein. There are clear differences in the distribution for the three forms of the protein. For the 2.3 mM oxidized form of the protein, 44 of 69 residues analyzed (64%) could be fit by model 1 containing only an S^2 term, and for the 0.48 mM oxidized sample, 49 of 66 residues analyzed (74%) could be fit by model 1 whereas only 23 out of 63 (37%) of the residues in the reduced form could be adequately modeled in this manner. For each of the following four models in which one or more additional parameters have been added to account for motion on different time scales, the reduced form of the protein has more residues even though the overall number of residues fit was less than for the oxidized forms. The values of the optimized model-free parameters are given in Table 1 for reduced and oxidized Grx-1. Plots of the optimized values of the model-free parameters for each form of the protein are shown in Figure 3.

Generalized Order Parameter (S^2). The mean value for the order parameter for the 2.3 mM oxidized protein is 0.91 ± 0.08, 0.86 ± 0.08 for the 0.48 mM oxidized sample, and 0.83 ± 0.07 for the reduced form of the protein. There is a significant difference in the generalized order parameter between the two different concentrations of the oxidized protein but no statistically significant difference between reduced Grx-1 and the lower concentration oxidized Grx-1. Plots of the differences in order parameters between reduced Grx-1 and 0.48 mM oxidized Grx-1 are given in Figure 4. Additionally, a plot of the differences in order parameters between the two oxidized forms of the protein is given in Figure 5.

Effective Correlation Time (τ_e). Figure 3 (panels D, E, and F) shows the values of the τ_e parameter for those residues in each form of the protein which required this parameter for an adequate fit. The anomalously high values of τ_e, obtained from the use of model 5, are not shown in Figure 3. Such anomalously high values of τ_e were also observed in the dynamics study of ribonuclease HI carried out by Palmer and co-workers (Mandel et al., 1995). As we have only measured T_1, T_2, and NOE values at a single field strength, the validity of these values cannot be assessed and they have been excluded from all comparisons. The pattern of residues requiring this parameter differs between the two forms of the protein as well as between the two concentrations of the oxidized protein. In addition, the number of residues requiring a τ_e parameter to obtain an adequate fit was larger for the reduced form than for either of the oxidized

Table 1: Backbone Dynamical Parameters for 2.3 mM Oxidized, Reduced, and 0.48 mM Oxidized *E. coli* Glutaredoxin[a]

residue	2°	model	S^2	S_f^2	τ_e (ps)	R_{ex} (s^{-1})	Γ_i
			2.3 mM oxidized *E. coli* glutaredoxin				
Met1							
Gln2	β_1	5	0.795 ± 0.040	0.909 ± 0.024	1744 ± 456		0.00
Thr3	β_1	1	0.907 ± 0.029				2.84
Val4	β_1	1	0.900 ± 0.025				3.39
Ile5	β_1	5	0.784 ± 0.057	0.931 ± 0.031	3085 ± 887		0.00
Phe6	β_1	1	0.911 ± 0.042				1.67
Gly7	β_1	1	0.945 ± 0.023				3.51
Arg8		1	0.950 ± 0.023				1.50
Ser9		1	0.954 ± 0.019				2.13
Gly10							
Cys11							
Pro12							
Tyr13	α_1						
Cys14	α_1	1	1.000 ± 0.014				0.74
Val15	α_1	2	0.913 ± 0.023		237 ± 123		3.65
Arg16	α_1	2	0.959 ± 0.024		160 ± 80		3.02
Ala17	α_1	1	0.985 ± 0.019				3.28
Lys18	α_1	3	0.950 ± 0.026			1.52 ± 0.53	0.011
Asp19	α_1	3	0.942 ± 0.017			1.29 ± 0.39	0.13
Leu20	α_1	1	0.962 ± 0.017				1.62
Ala21	α_1	1	0.983 ± 0.014				9.62
Glu22	α_1	1	0.952 ± 0.016				0.60
Lys23	α_1	3	0.917 ± 0.017			0.70 ± 0.34	0.36
Leu24	α_1	1	0.980 ± 0.017				3.74
Ser25	α_1	1	0.981 ± 0.014				3.91
Asn26	α_1	1	0.955 ± 0.015				0.23
Glu27	α_1	1	0.823 ± 0.016				7.75
Arg28	α_1	1	0.877 ± 0.013				8.63
Asp29		2	0.777 ± 0.015		89 ± 16		2.09
Asp30		5	0.758 ± 0.034	0.913 ± 0.021	1833 ± 359		0.00
Phe31		5	0.808 ± 0.034	0.904 ± 0.025	1204 ± 408		0.00
Gln32	β_2	5	0.741 ± 0.041	0.878 ± 0.024	2189 ± 804		0.00
Tyr33	β_2	2	0.920 ± 0.018		124 ± 55		0.002
Gln34	β_2	5	0.850 ± 0.045	0.988 ± 0.019	1859 ± 442		0.00
Tyr35	β_2						
Val36	β_2	1	0.881 ± 0.027				0.39
Asp37	β_2	1	0.877 ± 0.019				7.04
Ile38		1	0.968 ± 0.026				0.50
Arg39		1	0.975 ± 0.010				2.51
Ala40		1	0.852 ± 0.023				1.37
Glu41		1	0.935 ± 0.024				1.23
Gly42		1	0.903 ± 0.016				7.26
Ile43							
Thr44	α_2	1	0.947 ± 0.026				3.74
Lys45	α_2	1	0.987 ± 0.022				0.56
Glu46	α_2	1	0.983 ± 0.017				2.42
Asp47	α_2	1	0.946 ± 0.020				3.89
Leu48	α_2	1	0.972 ± 0.019				3.23
Gln49	α_2	1	0.967 ± 0.024				0.018
Gln50	α_2						
Lys51	α_2	1	0.946 ± 0.014				1.31
Ala52	α_2	3	0.928 ± 0.019			0.98 ± 0.38	0.046
Gly53	α_2	1	0.890 ± 0.016				6.58
Lys54		2	0.890 ± 0.012		101 ± 52		2.54
Pro55							
Val56		5	0.525 ± 0.021	0.840 ± 0.015	2260 ± 211		0.00
Glu57							
Thr58		3	0.829 ± 0.072			4.01 ± 1.65	2.13
Val59		1	1.000 ± 0.040				2.09
Pro60							
Gln61	β_3	1	0.922 ± 0.032				1.22
Ile62	β_3	1	0.894 ± 0.032				3.58
Phe63	β_3	2	0.865 ± 0.018		90 ± 32		1.30
Val64	β_3	1	0.891 ± 0.019				0.99
Asp65		1	0.981 ± 0.023				3.76
Gln66							
Gln67	β_4	2	0.911 ± 0.015		110 ± 46		0.004
His68	β_4	1	0.903 ± 0.019				1.60
Ile69	β_4	1	0.873 ± 0.034				1.59
Gly70		1	0.897 ± 0.026				2.56
Gly71	α_3	1	0.882 ± 0.032				6.23
Tyr72	α_3						
Thr73	α_3	3	0.968 ± 0.071			6.65 ± 2.69	0.03

Table 1: (Continued)

residue	2°	model	S^2	S_f^2	τ_e (ps)	R_{ex} (s^{-1})	Γ_i
			2.3 mM oxidized *E. coli* glutaredoxin				
Asp74	α_3	1	0.945 ± 0.048				1.57
Phe75	α_3	1	1.000 ± 0.044				3.68
Ala76	α_3	1	0.959 ± 0.024				1.82
Ala77	α_3	3	0.896 ± 0.019			1.64 ± 0.42	0.037
Trp78	α_3						
Val79	α_3	3	0.939 ± 0.027			1.43 ± 0.58	0.10
Lys80	α_3	3	0.895 ± 0.015			1.16 ± 0.33	0.01
Glu81	α_3	3	0.881 ± 0.015			1.08 ± 0.34	0.70
Asn82	α_3	1	0.875 ± 0.020				3.10
Leu83	α_3	2	0.849 ± 0.018		72 ± 29		1.86
Asp84							
Ala85							
			Reduced *E. coli* glutaredoxin				
Met1							
Gln2	β_1	1	0.811 ± 0.010				16.40
Thr3	β_1	1	0.837 ± 0.016				2.86
Val4	β_1	1	0.853 ± 0.015				5.69
Ile5	β_1	5	0.648 ± 0.066	0.872 ± 0.020	8038 ± 2252		0.00
Phe6	β_1						
Gly7	β_1	5	0.713 ± 0.039	0.906 ± 0.017	2258 ± 362		0.00
Arg8		2	0.912 ± 0.017		118 ± 50		0.012
Ser9		2	0.864 ± 0.011		106 ± 23		1.00
Gly10							
Cys11		1	0.775 ± 0.009				14.76
Pro12							
Tyr13	α_1	3	0.884 ± 0.031			4.10 ± 0.76	0.43
Cys14	α_1	3	0.864 ± 0.026			2.33 ± 0.58	0.16
Val15	α_1	3	0.867 ± 0.013			0.51 ± 0.23	2.23
Arg16	α_1	1	0.908 ± 0.009				2.97
Ala17	α_1	1	0.875 ± 0.008				17.20
Lys18	α_1	3	0.887 ± 0.010			0.44 ± 0.19	1.15
Asp19	α_1						
Leu20	α_1	3	0.873 ± 0.010			0.58 ± 0.21	0.53
Ala21	α_1	3	0.862 ± 0.010			0.76 ± 0.19	1.05
Glu22	α_1	1	0.862 ± 0.007				15.47
Lys23	α_1	2	0.895 ± 0.008		48 ± 20		0.059
Leu24	α_1	3	0.887 ± 0.011			0.59 ± 0.19	0.53
Ser25	α_1	3	0.842 ± 0.008			0.41 ± 0.15	0.27
Asn26	α_1	2	0.892 ± 0.010		78 ± 23		0.016
Glu27	α_1	2	0.733 ± 0.009		15 ± 8		3.01
Arg28	α_1						
Asp29							
Asp30		5	0.667 ± 0.029	0.864 ± 0.013	1670 ± 258		0.00
Phe31		2	0.806 ± 0.010		42 ± 12		0.83
Gln32	β_2	5	0.682 ± 0.048	0.850 ± 0.012	8322 ± 2187		0.00
Tyr33	β_2	1	0.865 ± 0.010				15.26
Gln34	β_2	5	0.771 ± 0.044	0.909 ± 0.017	2986 ± 873		0.00
Tyr35	β_2	1	0.835 ± 0.010				2.25
Val36	β_2	1	0.907 ± 0.015				2.14
Asp37	β_2	5	0.759 ± 0.036	0.864 ± 0.018	1483 ± 596		0.00
Ile38		1	0.906 ± 0.012				2.44
Arg39		1	0.869 ± 0.011				0.53
Ala40		1	0.807 ± 0.007				0.35
Glu41		4	0.752 ± 0.012		29 ± 10	1.04 ± 0.22	0.00
Gly42		2	0.749 ± 0.009		42 ± 8		0.32
Ile43		5	0.718 ± 0.030	0.821 ± 0.014	1743 ± 679		0.00
Thr44	α_2	5	0.684 ± 0.041	0.847 ± 0.015	4259 ± 881		0.00
Lys45	α_2	1	0.922 ± 0.011				4.84
Glu46	α_2						
Asp47	α_2	1	0.889 ± 0.008				2.38
Leu48	α_2	1	0.869 ± 0.010				2.08
Gln49	α_2	1	0.862 ± 0.008				4.44
Gln50	α_2	1	0.861 ± 0.007				3.90
Lys51	α_2	1	0.838 ± 0.008				0.51
Ala52	α_2	3	0.857 ± 0.009			1.08 ± 0.19	0.11
Gly53	α_2						
Lys54							
Pro55							
Val56							
Glu57							
Thr58							
Val59		4	0.759 ± 0.013		59 ± 11	0.45 ± 0.20	0.00
Pro60							

Table 1: (continued)

residue	2°	model	S^2	S_f^2	τ_e(ps)	R_{ex}(s^{-1})	Γ_i
			Reduced *E. Coli* glutaredoxin				
Gln61	β_3	2	0.883 ± 0.016		56 ± 42		2.19
Ile62	β_3	2	0.838 ± 0.018		51 ± 25		2.15
Phe63	β_3	1	0.859 ± 0.018				10.17
Val64	β_3						
Asp65		3	0.913 ± 0.021			1.35 ± 0.44	0.26
Gln66							
Gln67	β_4						
His68	β_4						
Ile69	β_4	1	0.854 ± 0.018				3.68
Gly70		1	0.861 ± 0.014				0.86
Gly71	α_3	5	0.681 ± 0.044	0.841 ± 0.016	2935 ± 605		0.00
Tyr72	α_3	2	0.805 ± 0.038		134 ± 45		2.51
Thr73	α_3	1	0.938 ± 0.013				12.13
Asp74	α_3	3	0.860 ± 0.011			0.55 ± 0.21	0.025
Phe75	α_3	3	0.854 ± 0.013			0.58 ± 0.26	0.58
Ala76	α_3						
Ala77	α_3	3	0.832 ± 0.009			1.02 ± 0.17	1.49
Trp78	α_3	4	0.804 ± 0.011		25 ± 11	0.94 ± 0.19	0.00
Val79	α_3	4	0.831 ± 0.012		44 ± 14	1.24 ± 0.21	0.00
Lys80	α_3	3	0.855 ± 0.008			0.87 ± 0.16	1.75
Glu81	α_3	3	0.821 ± 0.009			0.96 ± 0.18	0.82
Asn82	α_3	2	0.818 ± 0.012		35 ± 14		0.40
Leu83	α_3	2	0.748 ± 0.009		39 ± 9		0.11
Asp84							
Ala85							
			0.48 mM Oxidized *E. Coli* Glutaredoxin				
Met1							
Gln2	β_1	1	0.824 ± 0.019				2.64
Thr3	β_1	1	0.841 ± 0.029				2.71
Val4	β_1	1	0.874 ± 0.029				0.13
Ile5	β_1	1	0.848 ± 0.028				0.93
Phe6	β_1	1	0.787 ± 0.042				1.31
Gly7	β_1	2	0.818 ± 0.027		46 ± 18		2.60
Arg8		1	0.894 ± 0.024				1.11
Ser9		1	0.875 ± 0.020				3.39
Gly10							
Cys11							
Pro12							
Tyr13	α_1						
Cys14	α_1	1	0.966 ± 0.024				1.75
Val15	α_1	1	0.897 ± 0.023				0.33
Arg16	α_1	1	0.960 ± 0.020				3.16
Ala17	α_1	1	0.938 ± 0.027				1.65
Lys18	α_1	1	0.908 ± 0.025				0.86
Asp19	α_1	1	0.908 ± 0.017				0.19
Leu20	α_1	1	0.905 ± 0.019				0.39
Ala21	α_1	1	0.937 ± 0.017				3.34
Glu22	α_1	1	0.913 ± 0.016				3.03
Lys23	α_1	1	0.950 ± 0.015				8.88
Leu24	α_1	1	0.951 ± 0.021				9.90
Ser25	α_1	1	0.925 ± 0.015				3.39
Asn26	α_1	1	0.911 ± 0.017				1.90
Glu27	α_1	1	0.851 ± 0.019				7.50
Arg28	α_1						
Asp29		2	0.690 ± 0.015		65 ± 8		2.14
Asp30		5	0.701 ± 0.043	0.886 ± 0.030	1140 ± 336		0.00
Phe31		2	0.825 ± 0.017		114 ± 17		0.006
Gln32	β_2	5	0.720 ± 0.059	0.895 ± 0.030	2972 ± 688		0.00
Tyr33	β_2	1	0.885 ± 0.019				0.066
Gln34	β_2	1	0.871 ± 0.025				3.77
Tyr35	β_2						
Val36	β_2	1	0.826 ± 0.029				2.75
Asp37	β_2	1	0.816 ± 0.022				7.57
Ile38		1	0.923 ± 0.029				0.45
Arg39		1	0.934 ± 0.011				3.18
Ala40		1	0.807 ± 0.023				2.14
Glu41		1	0.906 ± 0.028				3.07
Gly42		1	0.787 ± 0.017				6.70
Ile43		1	0.821 ± 0.019				1.80
Thr44	α_2	1	0.862 ± 0.024				0.21
Lys45	α_2	1	0.948 ± 0.028				1.54
Glu46	α_2	1	0.900 ± 0.019				0.61
Asp47	α_2	1	0.898 ± 0.020				0.79

Table 1: (continued)

residue	2°	model	S^2	S_f^2	τ_e(ps)	R_{ex}(s^{-1})	Γ_i
			0.48 mM Oxidized *E. Coli* Glutaredoxin				
Leu48	α_2	1	0.893 ± 0.020				1.80
Gln49	α_2	2	0.836 ± 0.026		102 ± 28		0.79
Gln50	α_2						
Lys51	α_2	1	0.884 ± 0.016				0.24
Ala52	α_2	3	0.908 ± 0.030			1.07 ± 0.36	0.81
Gly53	α_2	2	0.866 ± 0.018		78 ± 30		0.016
Lys54							
Pro55							
Val56		5	0.445 ± 0.032	0.838 ± 0.023	2097 ± 200		0.00
Glu57							
Thr58		3	0.761 ± 0.097			2.51 ± 1.16	1.73
Val59		1	0.956 ± 0.047				8.64
Pro60							
Gln61	β_3	1	0.849 ± 0.036				0.31
Ile62	β_3	1	0.824 ± 0.032				0.76
Phe63	β_3						
Val64	β_3	1	0.858 ± 0.022				0.40
Asp65		3	0.871 ± 0.048			1.67 ± 0.67	0.31
Gln66							
Gln67	β_4						
His68	β_4	1	0.812 ± 0.018				7.00
Ile69	β_4	1	0.864 ± 0.037				0.074
Gly70		1	0.842 ± 0.028				0.25
Gly71	α_3	2	0.763 ± 0.033		66 ± 18		0.45
Tyr72	α_3						
Thr73	α_3						
Asp74	α_3	1	0.943 ± 0.051				0.82
Phe75	α_3	1	0.933 ± 0.060				0.18
Ala76	α_3	1	0.921 ± 0.029				1.76
Ala77	α_3	3	0.872 ± 0.030			0.96 ± 0.35	0.072
Trp78	α_3	3	0.860 ± 0.032			0.83 ± 0.38	0.30
Val79	α_3	1	0.944 ± 0.026				3.38
Lys80	α_3	3	0.868 ± 0.023			0.80 ± 0.29	0.21
Glu81	α_3	1	0.864 ± 0.016				2.48
Asn82	α_3	2	0.859 ± 0.022		92 ± 25		0.72
Leu83	α_3	5	0.712 ± 0.047	0.874 ± 0.030	1518 ± 373		0.00
Asp84							
Ala85							

[a] 2° indicates secondary structure, model is the model-free model employed to fit the relaxation data for each residue, as described in the text, $S^2 = S_f^2 S_s^2$ is the generalized order parameter, τ_e is the effective internal correlation time, R_{ex} is the value of the exchange broadening term, and Γ_i is the sum of squares error.

Table 2: Dynamical Parameters Optimized in the Final Model-Free Analysis

	2.3 mM oxidized	reduced	0.5 mM oxidized
number of resonances in calculation	69	63	66
model 1 (S^2 optimized)	44	23	49
model 2 (S^2, τ_e, optimized)	8	12	7
model 3 (S^2, R_{ex} optimized)	10	15	6
model 4 (S^2, τ_e, R_{ex} optimized)	0	4	0
model 5 (S_f^2, S^2, τ_e optimized)	7	9	4
optimized molecular correlation time, τ_m (ns)	7.95 ± 0.028	5.73 ± 0.021	6.37 ± 0.028

forms. The number of residues requiring a τ_e is reduced in the lower concentration oxidized sample relative to the higher concentration oxidized sample.

Conformational Exchange Parameter R_{ex}. The pattern of residues requiring an R_{ex} term is quite different for the reduced and oxidized forms of the protein (see Table 2). Only 10 and 6 residues required an R_{ex} term in the two oxidized forms of the protein whereas 19 residues required this term in the reduced form of the protein. Of these 19 residues, 12 have values of the exchange term < 1 s^{-1} which may or may not be significant, however the trend of more residues requiring this parameter in the reduced form than in the oxidized form is clear. The ΔR_{ex} plot in panel C of Figure 4 shows that there is a significant change in the R_{ex} parameter between the two forms of the protein for Cys14 which is located in the active site.

Two Time-Scale Spectral Density Functions. A total of seven residues in the 2.3 mM oxidized form (Gln2, Ile5, Asp30, Phe31, Gln32, Gln34, and Val56), four residues in 0.48 mM oxidized sample (Asp30, Gln32, Val56, and Leu83), and nine residues in the reduced form (Ile5, Gly7, Asp30, Gln32, Gln34, Asp37, Ile43, Thr44, and Gly71) required a two time-scale spectral density function. In all cases, the value of τ_e obtained was greater than 1 ns. For the reasons already mentioned above, these anomalously high values have not been included in any comparisons. In all three forms of the protein residues in β-strand 2 and the loop

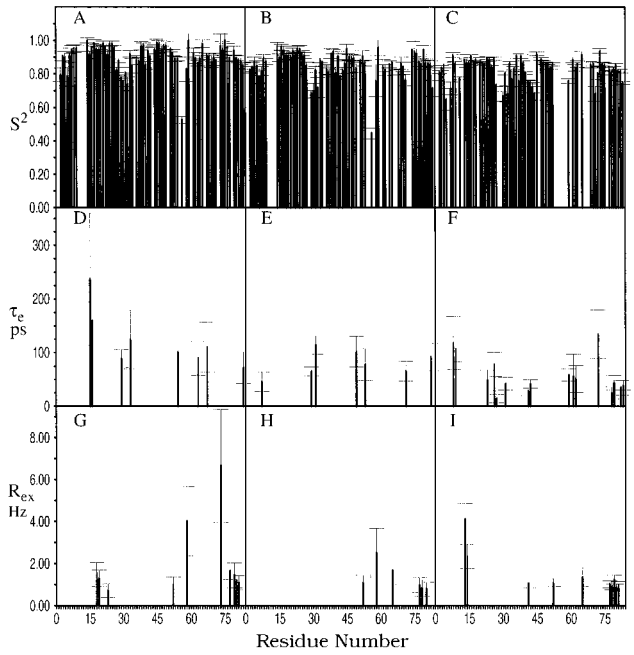

FIGURE 3: Calculated model-free parameters as a function of the resolved backbone NH groups in oxidized and reduced glutaredoxin: generalized order parameters, S^2, for 2.3 mM oxidized (A), 0.48 mM oxidized (B), and reduced (C) glutaredoxin; effective internal correlation times, τ_e, for 2.3 mM oxidized (D), 0.48 mM oxidized (E), and reduced (F) glutaredoxin; ^{15}N exchange broadening terms, R_{ex}, for 2.3 mM oxidized (G), 0.48 mM oxidized (H), and reduced (I) glutaredoxin. τ_e values for model 5 are not shown and only exchange broadening terms ≥ 1 s^{-1} are plotted.

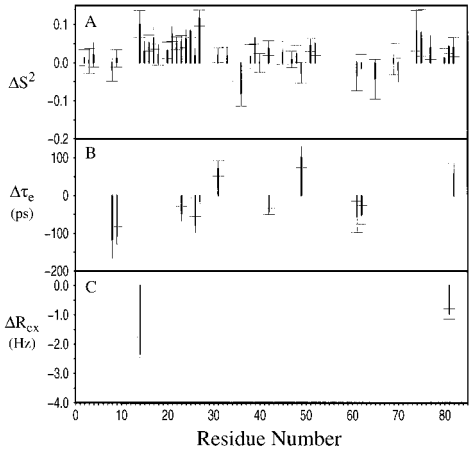

FIGURE 4: Calculated differences (0.48 mM oxidized − 2.3 mM reduced) in the model-free dynamics parameters (S^2, τ_e, R_{ex}) for resolved backbone NH groups between 0.48 mM oxidized and reduced glutaredoxin. Comparisons have not been made with any residues fit to the three parameter models (*i.e.*, models 4 or 5). Differences in the generalized order parameter, S^2 (panel A); differences in the effective internal correlation times, τ_e (panel B); differences in the ^{15}N exchange broadening terms where $\Delta R_{ex} > 1$ s^{-1} (panel C) are plotted.

leading to the N-terminal end of β-strand 2 required a two time-scale spectral density function.

DISCUSSION

Overall Correlation Time. The overall correlation times determined for the two forms of the protein differ significantly. The 5.73 ns value obtained for the reduced form of the protein is in agreement with previous determinations of the correlation times of proteins of this size by NMR (Kay et al., 1989; Stone et al., 1992; Kördel et al., 1992; Palmer et al., 1991; Clore et al., 1990a) and, in particular, is in good agreement with the 6.3 ns value obtained for the related but slightly larger *E. coli* thioredoxin protein (Stone et al., 1993). The 7.95 ns value obtained for the oxidized form of the protein is much larger than expected for a protein this size. On the basis of the calculations of the principal moments of inertia of each form, the shape of both forms of the protein is virtually identical. The most likely explanation involved aggregation of the oxidized form of the protein under the conditions employed for the NMR studies; therefore, we have carried out sedimentation equilibrium measurements to assess the oligomerization state of both forms of the protein. The reduced form of the protein was shown to be monomeric at all concentrations whereas the oxidized form exhibited a mass action association which could be modeled adequately as a weak ideal monomer−dimer equilibrium (data not shown). The model returned a monomer molecular mass of 9500 ± 500 kDa with an association constant of 1025 ± 200 M.

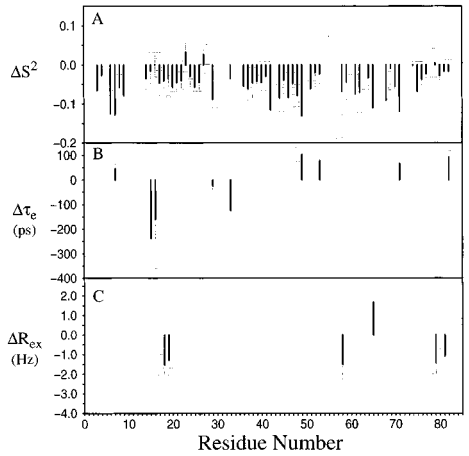

FIGURE 5: Calculated differences (0.48 mM oxidized − 2.3 mM oxidized) in the model-free dynamics parameters (S^2, τ_e, R_{ex}) for resolved backbone NH groups between 0.48 and 2.3 mM oxidized glutaredoxin. Comparisons have not been made with any residues fit to the three parameter models (*i.e.*, models 4 or 5). Differences in the generalized order parameter, S^2 (panel A); differences in the effective internal correlation times, τ_e (panel B); differences in the ^{15}N exchange broadening terms where $\Delta R_{ex} > 1$ s^{-1} (panel C) are plotted.

Because of the monomer−dimer equilibrium in the oxidized form of the protein, the measured relaxation parameters reflect a population-weighted average of the monomer and dimer forms. At the 2.3 mM concentration of protein utilized in these studies, the concentrations of monomer and dimer are 0.84 and 0.73 mM, so the majority of the protein is in the dimeric form. More importantly, dimerization has been shown to have a substantial effect on the dynamical parameters obtained from a model-free analysis (Schurr et al., 1994). The original model-free analysis of Lipari and Szabo (1982a,b) is strictly only applicable to a monomeric spherical molecule, so the rotational diffusion anisotropy associated with formation of the dimer distorts the values obtained from such an analysis. In particular, theoretical calculations showed that dimerization results in an overestimate of both the generalized order parameter, S^2, as well as the internal correlation time, τ_e (Schurr et al., 1994). For these reasons, we have collected a second set of relaxation data for the oxidized form of the protein at a concentration of 0.48 mM in addition to the data

originally collected at a 2.3 mM concentration. At 2.3 mM, the relative concentrations of monomer and dimer is 1.16/1, whereas at 0.48 mM this ratio increases to 3.3/1, thus ameliorating some of the distortion of the model-free parameters associated with making a model-free analysis on a system that has significant diffusional anisotropy. At 0.48 mM, the calculated correlation time for the oxidized protein is 6.37 ns, significantly down from the 7.95 ns value observed at the higher concentration and only 11% higher than the value obtained for the reduced protein. All comparisons of the oxidized protein to the reduced protein have been carried out with the data obtained at the lower concentration.

Backbone Dynamics of Oxidized Grx-1 at 2.3 and 0.48 mM. Plots of the S^2, τ_e, and R_{ex} values obtained from the 2.3 and 0.48 mM samples of oxidized Grx-1 are shown in Figure 3. Adequate fits were obtained for 66 residues in the 0.48 mM and for 69 residues in the 2.3 mM data. As shown in Table 2, the distribution of the residues among the models used for the fitting of the data are very similar for the two concentrations. Figure 5 shows the changes in S^2, τ_e, and R_{ex} terms for each residue observed upon going from 2.3 to 0.5 mM oxidized Grx-1. There is a clear reduction in the values of the order parameter upon reducing the concentration, as predicted by Schurr et al. (1994) for a system undergoing dimerization. The mean S^2 value for the 2.3 mM data is 0.91, and for the 0.48 mM data it is 0.86. There are nine residues that display a difference in τ_e with no obvious trend observed.

Measurements of T_1, T_2, and NOE at a single field strength do not permit the determination of model-free parameters for the monomer and dimer forms of the protein. Furthermore, the diffusional anisotropy of the dimer form would have to be assessed in order to be able to make a meaningful analysis of the dimer form of the protein. As the two forms of the protein are in rapid exchange on the NMR time scale, we are unable to employ the methods demonstrated by Bax and co-workers (Tjandra et al., 1995) or Wright and co-workers (Brüschweiler et al., 1995) to obtain a meaningful determination of the diffusional anisotropy in the dimer form of the protein.

N- and C-Termini. Most studies of protein dynamics have shown the N- and C-termini of proteins to be more disordered than the secondary structure elements with the C-terminus usually more mobile than the N-terminus. This observation also holds for both forms of Grx-1. Whereas the mean T_2 value determined for reduced Grx-1 is 134 ms, the values for Leu83, Asp84, and Ala85 show a sharp increase over this with values of 155, 262, and 369 ms. The mean NOE value for the reduced protein is 0.72 whereas the corresponding values for Leu83−Ala85 are 0.65, 0.27, and −0.45. Model-free parameters were not calculated for Asp84 and Ala85 due to inadequate fits of the T_1 and T_2 data. Virtually identical behavior is seen for these residues in the 0.48 and 2.3 mM oxidized forms. For the C-terminus, Leu83 falls more than 1 standard deviation below the mean S^2 value in the reduced and 0.48 mM oxidized forms. For the N-terminus, Gln2 and Thr3 falls within 1 standard deviation in both forms.

Backbone Dynamics of Reduced and Oxidized Grx-1. Grx-1 is an α/β protein with three helices and a four-stranded β-sheet as shown in Figure 6. Helices 1 and 3 run roughly parallel on one side of the β-sheet with helix 2 located on the other side of the sheet. The active site (Cys11−Cys14) is located at the N-terminal end of helix 1 as shown in Figure 6.

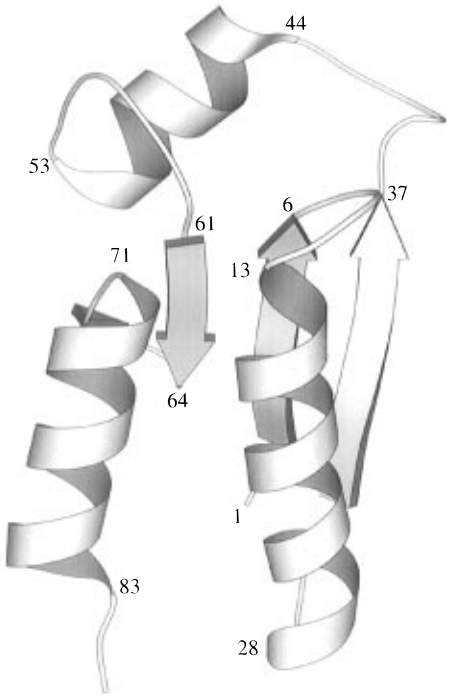

FIGURE 6: Ribbon representation of the backbone fold of *E. coli* glutaredoxin prepared using the program Molscript (Kraulis, 1991). Selected residue numbers are indicated on the structure.

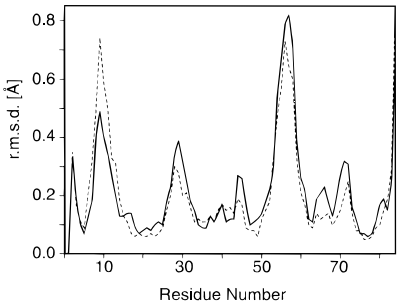

FIGURE 7: Local RMS derivative values for the backbone residues of oxidized and reduced Grx-1. Solid line: averaged values of the 190 pairwise comparisons among the 20 individual NMR conformers of oxidized Grx-1. Dashed line: same for the reduced protein.

The order parameters for the connecting loops in the protein show very different behavior depending on the loop. The loop connecting the first β-strand to the first helix (loop 11) and the loop connecting β-strand 2 to α-helix 2 both show order parameters close to or above the mean S^2 in both forms of the protein. The loop connecting the first α-helix to the second β-strand (loop 12) and the loop connecting the second α-helix to the third β-strand show order parameters well below the mean values for each form of the protein. For the reduced form, only a single residue (Val59) could be evaluated for loop 23, but its S^2 value is well below the mean. The higher mobility in these two loop regions correlates well with the higher backbone RMSD observed for these regions in the solution structures of the two forms of the protein (see Figure 7). On the basis of the observed order parameters for the residues in loop 11, the high RMSD in this region may be a reflection of the lower density of constraints obtained in this region of the protein rather than increased motion.

Table 3: Average Order Parameter Values for Secondary Structural Elements

structural element	resolved residues in 0.5 mM oxidized Grx-1 considered	oxidized S^2 average	resoled residues in reduced Grx-1 considered	reduced S^2 average
β_1	G2−G7	0.832 ± 0.030	Q2−I5, G7	0.772 ± 0.008
11	R8, S9	0.885 ± 0.010	R8, S9, C11	0.850 ± 0.070
α_1	C14−E27	0.923 ± 0.030	Y13−K18, L20−E27	0.867 ± 0.042
12	D29−F31	0.739 ± 0.075	D30−F31	0.737 ± 0.098
β_2	Q32−Q34, V36, D37	0.824 ± 0.065	Q32−D37	0.803 ± 0.082
22	I38−I43	0.863 ± 0.065	I38−I43	0.800 ± 0.074
α_2	T44−Q49, K51−G53	0.888 ± 0.032	T44−K45, D47−A52	0.848 ± 0.071
23	V56, T58, V59	0.721 ± 0.258	V59	
β_3	Q61, I62, V64	0.844 ± 0.018	Q61−F63	0.860 ± 0.023
β_4	H68, I69	0.838 ± 0.039	I69	
α_3	G71, D74−L83	0.867 ± 0.073	G71−F75, A77−L83	0.821 ± 0.063

Many previous studies have attempted to correlate the order parameter with elements of secondary structure with limited success. A previous study between the oxidized and reduced form of thioredoxin (Stone et al., 1993) found no significant correlation between order parameters and secondary structure type. Table 3 lists average order parameters for the various secondary structural elements as well as the loops connecting them in the two forms of Grx-1. As has been observed elsewhere (Farrow et al., 1994), the β-sheets for both forms of Grx-1 have lower order parameters than the helices. The average order parameters for the helices are 0.893 ± 0.028 and 0.845 ± 0.023 for the oxidized and reduced forms of the protein whereas for the residues of β_1−β_3 (only one residue was fit in the reduced form for β_4, so β_1−β_3 have been used for the comparison) the corresponding values are 0.833 ± 0.010 and 0.812 ± 0.045. The average values for the α-helices in reduced Grx-1 are comparable to those found in other studies (Mandel et al., 1995; Farrow et al., 1994; Kördel et al., 1992; Kay et al., 1989). The average values for α-helices 2 and 3 in the oxidized form are similar to values found in other studies whereas that for α-helix 1 is somewhat higher. The average β-sheet values for both forms of Grx-1 are similar to the values determined for β_1−β_4 in ribonuclease HI, 0.854 ± 0.011, 0.866 ± 0.006, 0.847 ± 0.005, and 0.846 ± 0.013 (Mandel et al., 1995), the large β-sheet of SH2 domain, 0.86 ± 0.04 (Farrow et al., 1994), the β-sheet of the glucose permease IIA domain, 0.81 ± 0.06 (Stone et al., 1992), and the β-sheets in staphylococcal nuclease, 0.86 ± 0.04 (Kay et al., 1989).

For helix 1 and helix 3, we have noted a decrease in the order parameter at the C-terminal end of the helix but no detectable difference in behavior at the N-terminus. Glu27 (0.85) in the oxidized form and Glu27 (0.73) in the reduced form at the end of helix 1 show reduced S^2 values relative to the remainder of the helix. In helix 3, the C-terminal residues 84 and 85 are quite flexible as already discussed and residues Lys80−Leu83 show a monotonic decrease in the order parameter consistent with this end of the helix being less stable.

β-strands 3 and 4 show reasonably uniform S^2 values throughout their lengths although only one residue was evaluated for β_4 in the reduced form so it is difficult to assess for this form of the protein. β-strand 1 shows a reasonably consistent behavior throughout with the exception of Ile5 which displays a depressed S^2 and required a two time-scale spectral density function to be fit in the reduced form of the protein (see Table 1). The N-terminal end of β-strand 2 presents an interesting pattern of dynamical parameters in the reduced form of the protein. Beginning with Gln32, there is a pattern of alternating low- and high-order parameters for the residues from Gln32 to Tyr35. The two residues showing reduced order parameters, Gln32 and Gln34, also required a two time-scale spectral density function to be adequately fit to the experimental data. This behavior is not observed in the oxidized form of the protein. Interestingly, these residues are hydrogen-bonded to residues in β-strand 1 which leads into the active site. β-strand 1 shows increased mobility in the reduced form of the protein relative to the oxidized form (see Table 2). This is not surprising considering its proximity to the active site residues. Interestingly, this increased mobility is apparently transmitted to the residues of β-strand 2 that are hydrogen-bonded to β-strand 1 resulting in their increased mobility.

Global Differences Between Oxidized and Reduced Glutaredoxin. As mentioned above, dimerization and the resulting diffusional anisotropy has been shown to distort the values of the dynamical parameters obtained from a model-free analysis of relaxation data (Schurr *et al.*, 1994). In order to counter this, we have collected the data for the oxidized protein at a lower concentration (0.48 mM) in order to reduce the effects of dimerization on the derived dynamical parameters. The mean S^2 values for the 2.3 mM oxidized and reduced proteins are 0.91 and 0.83, respectively; thus, the S^2 values do appear artificially high for the oxidized form. The corresponding value for the 0.48 mM oxidized protein is 0.86, a significant improvement over the 2.3 mM value but still higher than that obtained for the reduced protein, suggesting there may be some influence of the dimerization on the dynamical parameters. All comparisons between the oxidized and reduced proteins have been carried out using the oxidized data obtained at 0.48 mM. Any comparison between the two forms of the protein must bear this in mind. In addition, we have only collected T_1, T_2, and NOE values at a single field strength, so the statistical protocol we have employed cannot be used to evaluate the validity of models with three dynamical parameters, namely models 4 and 5. The residues fit with model 5, in particular, display anomalously high values of τ_e, which was also observed in the dynamics study of Ribonuclease HI carried out by Palmer and co-workers (Mandel *et al.*, 1995). The necessity of employing additional parameters to get an adequate fit is an indication of additional motion for these residues; however, the reliability of the numerical values obtained for the dynamical parameters cannot be evaluated. For this reason, when making comparisons between forms of the protein, we have not included comparisons for any residues in which models 4 or 5 have been employed for the fitting of the data.

With these caveats in mind, the differences in the dynamical parameters between the oxidized and reduced proteins present a very interesting picture. As shown in Table 2, 49 of 66 residues (74%) in the oxidized form could be fit by model 1 optimizing only S^2 whereas only 23 of 63 residues (37%) in the reduced form could be fit with this model. Dimerization is predicted to *increase* the observed τ_e values in particular (Schurr *et al.*, 1994). The dimerization of the oxidized form should therefore *decrease* the number of residues fit with model 1. For this reason, we believe this difference in model distribution between the two forms of the protein to be the result of a real difference in the mobilities of the two proteins. The reduced protein also has significantly more residues requiring an R_{ex} exchange term (models 3 and 4) or a two time-scale spectral density function (model 5) also implying significantly more mobility in the reduced form. Although the magnitude of the order parameters obtained for the oxidized form must be interpreted with caution due to the increases associated with dimerization, the higher mean S^2 value for the oxidized protein (0.86) relative to the reduced protein (0.83) as also consistent with higher mobility in the reduced form of the protein.

The redox potential of a disulfide containing protein is directly linked to the thermodynamic stability of the reduced and oxidized forms of the protein as has been very elegantly confirmed experimentally for several proteins in the thioredoxin superfamily to which Grx-1 belongs (Lin & Kim, 1989; Wunderlich *et al.*, 1993; Zapun *et al.*, 1993). Recently, the stability of the reduced and oxidized forms of Grx-1 has been reexamined using GdmCl denaturation monitored by circular dichroism spectroscopy (Åslund, 1996). This study clearly showed the oxidized form of the protein to be more stable than the reduced form by 1.0 kcal/mol in good agreement with the measured redox potential for the protein. On the continuum from unfolded to a fully folded protein, there is a dramatic decrease in the mobility of the residues in a protein; thus, we associate decreased mobility to a certain extent with increased stability. Although local regions of a polypeptide chain may contribute to an overall favorable free energy by being mobile and thereby increasing the entropy of the protein, the bulk of a protein becomes more rigid upon folding to form a stable tertiary structure. This loss of mobility is essential for the forces driving protein folding, expulsion of water from the hydrophobic core, van der Waals forces, etc., to be maximized. To the extent that this generalization is true, the dynamical behavior of the reduced and oxidized proteins correlates well with their thermodynamic stabilities, with the less stable reduced form of the protein displaying a great deal more motion on several time scales. Since only subtle structural differences have been discerned between the two forms of the protein, it appears that the dynamics plays an important role in determining the thermodynamic stability and thereby the redox potential of Grx-1. Figure 4 shows the differences in dynamical parameters between residues in the oxidized and reduced proteins. As mentioned above, differences in the dynamical parameters must be interpreted with care due to the dimerization of the oxidized form. However, a number of trends are quite clear. Fully half of the residues displaying significant differences in S^2 between the reduced and oxidized forms are located in helix 1, which contains the active site disulfide at its N-terminus. Clearly, the redox state of the disulfide has a profound influence on the dynamic behavior of helix 1. Significant differences are also observed for Asp74 and Phe75, which are located at the N-terminal end of helix 3, which is in close spatial proximity to the active site. Additional smaller differences are observed further down this helix apparently transmitted from the N-terminal residues. Only one residue, Val36, shows a statistically significant increase in order parameter upon going from the reduced to the oxidized form. Twenty of the twenty-two residues showing a statistically significant difference in S^2 between the reduced and oxidized forms have a $\Delta S^2 > 0.03$. As this is the difference between the mean S^2 values for the reduced and oxidized proteins, we believe this trend to be real and not an artifact of comparison with a dimer form. Figure 4 also shows the differences observed in the τ_e and R_{ex} terms between the oxidized and reduced proteins. The trend is clearly to increasing mobility in the reduced form relative to the oxidized form. Eight of the eleven τ_e differences between the two forms arise from a larger value of τ_e in the reduced protein. The two largest differences in τ_e arise for Arg8 and Ser9. Arg8 and Ser9 are in β-strand 1 leading into the active site. All the differences in R_{ex} terms arise from a larger value of R_{ex} for the reduced protein. A significant increase in R_{ex} is observed for Cys14 which is part of the active site loop. It thus appears that the many of the differences in dynamical behavior for the two forms of Grx-1 are localized to the active site and helices 1 and 3.

Changes in dynamical behavior in helices 1 and 3 may be of significant functional significance, since this is the presumed surface for the interaction of Grx-1 with its protein disulfide substrates. Recognition processes involving protein−ligand or protein−protein binding require protein flexibility for the conformational changes necessary for function to take place (Bennett & Huber, 1983; Ringe & Petsko, 1985; Brooks *et al.*, 1988). Previously, a reduction in the solvent accessible surface area for those residues located on this presumed interaction surface has been noted upon going from reduced to oxidized Grx-1 (Xia *et al.*, 1992). On the basis of this difference, it was proposed that the reduced form of the protein existed in an "open" conformation that allows it to interact more favorably with its protein disulfide substrates whereas the oxidized form was less accessible leading to dissociation from the protein disulfide substrate. This picture fits well with the observed dynamic behavior of the two forms of the protein where the necessary flexibility for efficient binding is present in the reduced form of Grx-1 but absent in the oxidized form.

Dynamics Changes in the Vicinity of the Active Site. Perusal of the dynamical parameters obtained for residues in the vicinity of the active site yields a number of interesting patterns. Active site dynamical parameters were obtained for Cys11, Tyr13, and Cys14 in the reduced form but only for Cys14 in the oxidized form. The NHs of Cys11 and Tyr13 have never been observed for the oxidized form. For the reduced form, both Cys14 and Tyr13 show S^2 values within 1 standard deviation of the mean whereas Cys11 gives a value of 0.775 which is well below the mean S^2 value for the reduced protein (0.83). Cys14 in the oxidized form of the protein yielded an S^2 value of 0.966, one of the highest values observed for any residue in either form of the protein, consistent with a very rigid active site in the oxidized form of the protein that becomes much more flexible upon reduction. Additionally, Tyr13 and Cys14 in the reduced form require an R_{ex} exchange-broadening term to obtain an

adequate fit indicating motion on the micro−millisecond time scale in addition to the increased motion on the pico−nanosecond time scale seen for Cys14. As seen in Figure 4, there are a couple of changes in the value of the R_{ex} term between the two forms of the protein. Cys14 shows a significant decrease in the R_{ex} term for this residue, again indicating that reduction results in increased motion on the micro−millisecond time scale as well as the nano−picosecond time scale. As mentioned above and with the caveat already mentioned about this comparison, fully half of the changes in S^2 observed are found in helix 1 in which the active site is located at the N-terminal end. These changes uniformly indicate increased motion in the reduced protein. Val59 is located in an extended element leading from α_2 to β_3 and has been shown to be a part of the glutathione binding site on Grx-1 (Bushweller *et al.*, 1994). Val59 required both a τ_e and an R_{ex} term to obtain an adequate fit in the reduced form where an S^2 value of 0.759 was obtained. Since this residue was fit with model 4, it has not been included in the previous comparisons. For the oxidized form, Val59 required only an S^2 term for adequate fitting and an S^2 value of 0.956, one of the highest values observed for any residue in either form of the protein, was obtained. Again, these results show a high rigidity for the active site and those residues in proximity to the active site in the disulfide form of Grx-1 that is significantly diminished upon reduction of the disulfide. Residues at the N-terminal end of α_3 have been identified as playing a role in the binding of GSH (Bushweller *et al.*, 1994) and are spatially close to the active site. As mentioned previously, Asp74 and Phe75 at the N-terminal end of α_3 show significant changes in S^2 that are again consistent with a more rigid surface in the active site region of the protein that becomes significantly more flexible in the reduced protein. Clearly, there are significant changes in both pico−nanosecond and micro−millisecond time-scale motions for those residues in the active site and spatially close to the active site. These changes are likely to be quite significant since these residues have been shown to play a role in binding GSH (Bushweller *et al.*, 1992) and undoubtedly also play a role in the binding of Grx-1 to its protein disulfide substrates.

CONCLUSIONS

In conclusion, determination of dynamical parameters for the reduced and oxidized forms of Grx-1 has revealed a difference in dynamic behavior between the two forms of the protein. The reduced form of the protein shows increased motion on both pico−nanosecond as well as micro−millisecond time scales relative to the oxidized form which correlates well with the greater thermodynamic stability of the oxidized form of Grx-1. In addition, significant differences in motion on the pico−nanosecond as well as micro−millisecond time scales are observed between the two forms of the protein for those residues spatially close to the active site. These differences are likely to play an important role in the binding of glutaredoxin to glutathione as well as to its protein disulfide substrates.

ACKNOWLEDGMENT

We are grateful to Dr. Arthur G. Palmer, III, and Dr. Mikael Akke for providing the Modelfree (version 3.1) software, awk shell scripts, and many helpful discussions. We thank Mr. Wayne Casey for his help in maintaining the NMR spectrometer.

SUPPORTING INFORMATION AVAILABLE

Table providing the values and uncertainties, for each residue, of the experimentally determined T_1, T_2, and NOE data (6 pages). Ordering information is given on any current masthead page.

REFERENCES

Abragam, A. (1961) *Principles of Nuclear Magnetism*, Clarendon Press, Oxford.
Ahn, B.-Y., & Moss, B. (1992) *Proc. Natl. Acad. Sci. U.S.A. 89*, 7060−7064.
Åslund, F. (1996) Ph.D. Thesis, Medical Nobel Institute for Biochemistry, Karolinska Institutet, Stockholm, Sweden.
Åslund, F., Ehn, B., Miranda-Vizuete, A., Pueyo, C., & Holmgren, A. (1994) *Proc. Natl. Acad. Sci. U.S.A. 91*, 9813−9817.
Bartels, C., Xia, T.-H., Billeter, M., Güntert, P., & Wüthrich, K. (1995) *J. Biomol. NMR 5*, 1−10.
Bennet, W. S., & Huber, R. (1983) *CRC Crit. Rev. Biochem. 15*, 291−384.
Björnberg, O., & Holmgren, A. (1991) *Protein Expression Purif. 2*, 287−295.
Brooks, C. L., Karplus, M., & Pettitt, B. M. (1988) *Adv. Chem. Phys. 71*, 1−259.
Brüschweiler, R., Liao, X., Wright, P. E. (1995) *Science 268*, 886−889.
Bushweller, J. H., Åslund, F., Wüthrich, K., & Holmgren, A. (1992) *Biochemistry 31*, 9288−9293.
Bushweller, J. H., Billeter, M., Holmgren, A., & Wüthrich, K. (1994) *J. Mol. Biol. 235*, 1585−1597.
Cantor, C. R., & Schimmel, P. R. (1980) *Biophysical Chemistry*, p 563, Freeman, San Francisco.
Chandrasekhar, K., Krause, G., Holmgren, A., & Dyson, H. J. (1991) *FEBS Lett. 284*, 178−183.
Clore, G. M., Driscoll, P. C., Wingfield, P. T., & Gronenborn, A. M. (1990a) *Biochemistry 29*, 7387−7401.
Clore, G. M., Szabo, A., Bax, A., Kay, L. E., Driscoll, P. C., & Gronenborn, A. M. (1990b) *J. Am. Chem. Soc. 112*, 4989−4991.
Dyson, H. J., Gippert, G. P., Case, D. A., Holmgren, A., & Wright, P. E. (1990) *Biochemistry* 29, 4129−4136.
Eklund, H., Ingelman, M., Söderberg, B.-O., Uhlin, T., Nordlund, P., Nikkola, M., Sonnerstam, U., Joelson, T., & Petratos, K. (1992) *J. Mol. Biol. 228*, 596−618.
Farrow, N. A., Muhandiram, R., Singer, A. U., Pascal, S. M., Kay, C. M., Gish, G., Shoelson, S. E., Pawson, T., Forman-Kay, J. D., & Kay, L. E. (1994) *Biochemistry 33*, 5984−6003.
Forman-Kay, J, D., Clore, G. M., Wingfield, P. T., & Gronenborn, A. M. (1991) *Biochemistry 30*, 2685−2698.
Gan, Z.-R., & Wells, W. W. (1987) *J. Biol. Chem. 262*, 6704−6707.
Gan, Z.-R., Polokoff, M. A., Jacobs, J. W., & Sordana, M. K. (1990) *Biochem. Biophys. Res. Commun. 168*, 944−951.
Güntert, P., Dötsch, V., Wider, G., & Wüthrich K. (1992) *J. Biomol. NMR 2*, 619−629.
Hiyama, Y., Niu, C.-H., Silverton, J. V., Bavoso, A., & Torchia, D. A. (1988) *J. Am. Chem. Soc., 110*, 2378−2383.
Holmgren, A. (1976) *Proc. Natl. Acad. Sci. U.S.A. 73*, 2275−2279.
Holmgren, A. (1979a) *J. Biol. Chem. 254*, 3664−3671.
Holmgren, A. (1979b) *J. Biol. Chem. 254*, 9113−9119.
Holmgren, A. (1985) *Annu. Rev. Biochem. 54*, 237−271.
Höög, J.-O., Jörnvall, H., Holmgren, A., Carlquist, M., & Persson, M. (1983) *Eur. J. Biochem. 136*, 223−232.
Hopper, S., Johnson, R. S., Vath, J. E., & Biemann, K. (1989) *J. Biol. Chem. 264*, 20438−20447.
Jeng, M. F., Campbell, A. P., Begley, T., Holmgren, A., Case, D. A., Wright, P. E., & Dyson, H. J. (1994) *Structure 2*, 853−868.
Johnson, G. P., Goebel, S. J., Perkus, M. E., Davis, S. W., Winslow, J. P., & Paoletti, E. (1991) *Virology 181*, 378−381.
Johnson, M. L., Correia, J. J., Yphantis, D. A., & Halvorson, H. R. (1981) *Biophys. J. 36*, 575−588.

Katti, S. K., LeMaster, D. M., & Eklund, H. (1990) *J. Mol. Biol. 212*, 167−184.
Katti, S. K., Robbins, A. H., Yang, Y., & Wells, W. W. (1995) *Protein Sci. 4*, 1998−2005.
Kay, L. E., Torchia, D. A., & Bax, A. (1989) *Biochemistry 28*, 8972−8979.
Kay, L. E., Keifer, P., & Saarinen, T. (1992) *J. Am. Chem. Soc. 114*, 10663−10665.
Kharakoz, D. P. (1989) *Biophys. Chem. 34*, 115−125.
Klintrot, I.-M., Höög, J.-O., Jörnvall, H., Holmgren, A., & Luthman, M. (1984) *Eur. J. Biochem. 144*, 417−423.
Kördel, J., Skelton, N. J., Akke, M., Palmer, A. G., III, & Chazin, W. J. (1992) *Biochemistry 31*, 4856−4866.
Kraulis, P. (1991) *J. Appl. Crystallogr. 24*, 946−950.
Laue, T. M. (1992) *Short Column Sedimentation Equilibrium Analysis for Rapid Characterization of Macromolecules in Solution*, Technical Information DS-835 Beckman Instruments Inc., Palo Alto, CA.
Laue, T. M. (1995) *Methods Enzymol. 259*, 427−452.
Laue, T. M., Shah, B. D., Ridgeway, T. M., & Pelletier, S. L. (1992) in *Analytical Ultracentrifugation in Biochemistry and Polymer Science* (Harding, S. E., Rowe, A. J., & Horton, J. C., Eds.) pp 90−125, Royal Society of Chemistry, London.
Lin, T.-Y., & Kim, P. S. (1989) *Biochemistry 28*, 5282−5287.
Lipari, G., & Szabo, A. (1982a) *J. Am. Chem. Soc. 104*, 4546−4559.
Lipari, G., & Szabo, A. (1982b) *J. Am. Chem. Soc. 104*, 4559−4570.
Luthman, M., & Holmgren, A. (1982) *J. Biol. Chem. 257*, 6686−6690.
Luthman, M., Eriksson, S., Holmgren, A., & Thelander, L. (1979) *Proc. Natl. Acad. Sci. U.S.A. 76*, 2158−2162.
Mandel, A., Akke, M., & Palmer, A. G., III (1995) *J. Mol. Biol. 246*, 144−163.
Mårtensson, J., & Meister, A. (1991) *Proc. Natl. Acad. Sci. U.S.A. 88*, 4656−4660.
Minakuchi, K., Yabushita, T., Masumura, T., Ichihara, K., & Tanaka, K. (1994) *FEBS Lett. 337*, 157−160.
Padilla, C. A., Martínez-Galisteo, E., Bárcena, J. A., Spyrou, G., & Holmgren, A. (1995) *Eur. J. Biochem. 227*, 27−34.
Palmer, A. G., III (1993) *Curr. Opin. Biotechnol. 4*, 385−391.
Palmer, A. G., III Rance, M., & Wright, P. E. (1991) *J. Am. Chem. Soc. 113*, 4371−4380.
Qin, J., Clore, G. M., & Gronenborn, A. M. (1994) *Structure 2*, 503−522.
Ringe, D., & Petsko, G. (1985) *Prog. Biophys. Mol. Biol. 45*, 197−235.
Schurr, J. M., Babcock, H. P., & Fujimoto, B. S. (1994) *J. Magn. Reson., Ser. B 105*, 211−224.
Skelton, N. J., Palmer, A. G., III, Akke, M., Kördel, J., Rance, M., & Chazin, W. J. (1993) *J. Magn. Reson., Ser. B 102*, 253−264.
Sklenar, V., Torchia, D. A., & Bax, A. (1987) *J. Magn. Reson. 73*, 375−379.
Sodano, P., Xia, T.-H., Bushweller, J. H., Björnberg, O., Holmgren, A., Billeter, M., & Wüthrich, K. (1991) *J. Mol. Biol. 221*, 1311−1324.
Starovasnik, M. A., Blackwell, T. K., Laue, T. M., Weintraub, H., & Klevit, R. E. (1992) *Biochemistry 31*, 9891−9903.
Stone, M. J., Fairbrother, W. J., Palmer, A. G., III, Reizer, J., Saier, M. H., Jr., & Wright, P. E. (1992) *Biochemistry 31*, 4394−4406.
Stone, M. J., Chandrasekhar, K., Holmgren, A., Wright, P. E., & Dyson, H. J. (1993) *Biochemistry 32*, 426−435.
Tjandra, N., Feller, S. E., Pastor, R. W., & Bax, A. (1995) *J. Am. Chem. Soc. 117*, 12562−12566.
Venable, R. M., & Pastor, R. W. (1988) *Biopolymers 27*, 1001−1014.
Wagner, G. (1993) *Curr. Opin. Struct. Biol. 3*, 748−753.
Wells, W. W., Peng Xu, D., Yang, Y., & Rocque, P. A. (1990) *J. Biol. Chem. 265*, 15361−15364.
Wunderlich, M., Jaenicke, R., & Glockshuber, R. (1993) *J. Mol. Biol. 233*, 559−566.
Xia, T.-H., Bushweller, J. H., Sodano, P., Billeter, M., Björnberg, O., Holmgren, A., & Wüthrich, K. (1992) *Protein Sci. 1*, 310−321.
Yphantis, D. A. (1960) *Ann. NY Acad. Sci. 88*, 586−601.
Yphantis, D. A. (1964) *Biochemistry 3*, 297−317.
Zapun, A., Bardwell, J. C. A., & Creighton, T. E. (1993) *Biochemistry 32*, 5083−5092.
Ziegler, D. M. (1985) *Annu. Rev. Biochem. 54*, 305−329.

BI962181G